

Article

# Methylene Blue Optical Fiber Sensor Filled with Calcium Alginate Hydrogel

Ning Wang \*, Wenting Liu, Shiqi Liu, Liang Xu, Longjiao Wang, Ming He and Dong Fang

College of Science, China University of Petroleum (East China), No.66 Changjiang West Road, Qingdao 266580, China; s21090091@s.upc.edu.cn (W.L.); s22090002@s.upc.edu.cn (S.L.); z22090009@s.upc.edu.cn (L.X.); s23090002@s.upc.edu.cn (L.W.); z23090020@s.upc.edu.cn (M.H.); 2109030203@s.upc.edu.cn (D.F.)

\* Correspondence: qfwangning@upc.edu.cn

**Abstract:** As it is a typical dye pollutant in water, methylene blue detection is important to health and environmental safety. A kind of methylene blue optical fiber sensor was successfully fabricated, which was highly sensitive, responded linearly, was easy to manufacture and was low cost. The sensor was composed of a capillary glass tube, single-mode fiber and calcium alginate hydrogel. The interference spectrum of the optical fiber F–P cavity successfully responded to the methylene blue solution. The response sensitivity of 2.46 nm/(mg/L) was obtained with the typical sensor with a 39.18  $\mu\text{m}$  cavity length. The linearity of the experiment curve was 0.99247. Furthermore, the influence of sodium alginate concentrations on sensitivity was also investigated. The results showed that the sodium alginate concentration had an optimum value. In addition, the dynamic response characteristic was tested. A 25 s response time was obtained with testing using a typical sensor, which showed a fast response time. The sensor has the potential to be applied to online methylene blue detection.

**Keywords:** methylene blue; calcium alginate hydrogel; Fabry–Perot; optical fiber sensor



**Citation:** Wang, N.; Liu, W.; Liu, S.; Xu, L.; Wang, L.; He, M.; Fang, D. Methylene Blue Optical Fiber Sensor Filled with Calcium Alginate Hydrogel. *Photonics* **2023**, *10*, 1251. <https://doi.org/10.3390/photonics10111251>

Received: 26 September 2023  
Revised: 9 November 2023  
Accepted: 9 November 2023  
Published: 12 November 2023



**Copyright:** © 2023 by the authors. Licensee MDPI, Basel, Switzerland. This article is an open access article distributed under the terms and conditions of the Creative Commons Attribution (CC BY) license (<https://creativecommons.org/licenses/by/4.0/>).

## 1. Introduction

Dyes are one of the typical emerging pollutants of water from industrial effluents. As a common dye compound, methylene blue (MB) is widely used in textile industrial dyes, laboratory dyes, medical system drugs and other fields [1–3]. Methylene blue and its metabolites in the human and animal body have certain toxicities [4] and mutagenic effects of cancer [5]. Louis M. Rifici showed that methylene blue was harmful to larval fathead minnows (*Pimephales promelas*) when the concentration was 2.1 mg/L [6]. In addition, methylene blue in water cannot be biodegraded but can be accumulated in organisms through bioenrichment, which will cause serious water pollution and ultimately threaten human health and ecological environmental safety [7,8].

The main measurement methods of methylene blue include the surface-enhanced Raman method (SERS) [9,10], high-performance liquid chromatography (HPLC) [11], immunoassay, electrochemical method [12,13], colorimetry [14], ultra-high performance liquid chromatography–tandem mass spectrometry [15] and spectrophotometry [16]. Many measurement methods have complex processing, low sensitivity and some other problems. In 2022, Elumalai Ashok Kumar [17] prepared a surface-enhanced Raman spectroscopy active substrate composed of Au nanoparticles (NP) on Cu<sub>2</sub>O microspheres using polyols and photochemical methods. The analytical enhancement factor for the effective measurement of methylene blue (MB) was  $2.55 \times 10^{12}$ , and the measurement limit was as low as  $2.36 \times 10^{-13}$  M. In 2021, Moustafa Zahran [18] first developed a new electrochemical amplification sensor using silver Arabic colloidal nanoparticles (AgNPs). The linear ranges of sensors based on AgNP, methylene blue monomer and poly methylene blue oxidation are 1–20  $\mu\text{g/L}$ , 0.1–10  $\mu\text{g/L}$  and 1–15  $\mu\text{g/L}$ , respectively. In 2020, Takuya Okazaki et al. [19]

proposed an electrochemical long-period fiber grating (LPFG) sensor with a high methylene blue response sensitivity and a sensor that responds to a wide concentration range from 0.001 mM to 1 mM.

Compared with the above methods, optical fiber sensing technology in the field of water pollution measurement has the advantages of a high detection limit, simple production process, low cost, anti-electromagnetic interference, real-time online measurement, high temperature and corrosion resistance, which can be applied to a variety of harsh environments [20–22]. In recent years, some reports about optical fiber measurement of water pollutants have been shown [23–26]. In 2013, Ji Luo et al. [27] successfully prepared a silver nanoparticle-modified evanescent field optic fiber sensor based on the MEMS microchannel chip. In the methylene blue concentration range from 0 to 0.4  $\mu\text{mol/mL}$ , the sensor response was linear ( $R^2 = 0.9496$ ). A concentration change of 0.1  $\mu\text{mol/mL}$  resulted in an absorbance change of 0.402 dB. In 2020, Kenza Azil et al. [28] studied an unclad optic fiber sensor based on evanescent wave absorption to monitor water pollution caused by methylene blue, with a wide sensitive range of methylene blue concentrations. The optical sensing method for methylene blue still needs to be deeply researched because of its inadequate investigation.

For many measurement methods of methylene blue at present, there are some problems, such as complex preprocessing, expensive instruments, long measurement time, nonlinear response and low sensitivity. Therefore, more convenient, fast and sensitive sensors need to be explored, especially the optical fiber sensor. This paper designed an optical fiber Fabry–Perot (F–P) sensor structure to measure the concentration of methylene blue solution, which is composed of a capillary glass tube, single-mode fiber and sensitive film (calcium alginate). It was easy to fabricate with a simple and low-cost structure. The methylene blue concentration was measured with the fiber F–P cavity interference spectrum. It was demonstrated that the sensor had a good linear response and high response sensitivity, and its sensitivity influence factors and dynamic response characteristics were also investigated. The research results are very helpful to realize the online monitoring of methylene blue water pollution.

## 2. Materials and Methods

### 2.1. Sensor Structure and Principle

The optical fiber sensor structure is shown in Figure 1. The sensor is composed of a capillary glass tube, single-mode fiber and calcium alginate-sensitive film. Figure 1a is the schematic diagram of the structure, Figure 1b is the schematic diagram of the two-reflection model, and Figure 1c is the real photo of the sensor. For sensor fabrication, firstly, one end of the single-mode optical fiber is connected to the Micron Optics SM125 optical fiber sensor analyzer, and the other end is peeled off with a wire stripper. After cleaning with alcohol, the end face is cut flat with an optical fiber cutter and then probed into the glass capillary tube. The position of the end face of the single-mode optical fiber is manually adjusted and monitored using a microscope. Until the annular end face of the glass capillary tube is flush with the end face of the single-mode fiber, the other end face of the capillary tube is sealed and fixed with 502 glue to fix the position. Then, we attach some sodium alginate to the fiber end to form the F–P cavity structure with the single-mode fiber and the sensitive film. We carefully adjust the cavity until the SM125 optical fiber sensing analyzer shows a good interference spectrum. Then, the calcium alginate hydrogel film in calcium chloride solution is fully solidified after a period until the SM125 interference spectrum is stable. Finally, we take off the sensor head and put it in the experimental environment for follow-up experiments.

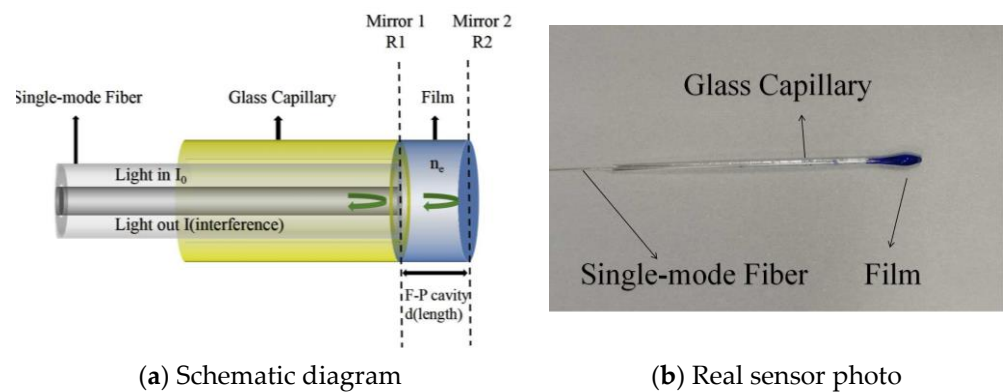


Figure 1. Sensor structure figure.

The sensor structure is shown in Figure 1a. The single-mode fiber and the calcium alginate-sensitive film constitute two cavity mirrors of the F–P cavity, forming the interference structure. The optical path difference between the two reflected beams can be expressed as [29]

$$L = 2n_e d \tag{1}$$

As Figure 1a showed,  $n_e$  is the effective refractive index of the calcium alginate hydrogel material, and  $d$  represents the distance between the two reflection ends (i.e., the cavity length of the F–P cavity). The interference intensity formed by the two reflected waves can be expressed as [30]

$$I = I_0 \left[ R_1 + R_2 + 2\sqrt{R_1 R_2} \cos \left( \frac{2\pi L}{\lambda} + \phi_0 \right) \right] \tag{2}$$

where  $I_0$  is the incident light intensity,  $R_1$  and  $R_2$  are the reflectance of each reflector,  $\lambda$  represents the wavelength of the light source, and  $\phi_0$  is the phase constant.

The optical path difference change in the F–P cavity caused by the change in the external environment is [29]

$$\Delta L = 2(\Delta n_e d + n_e \Delta d) = L \left( \frac{\Delta n_e}{n_e} + \frac{\Delta d}{d} \right) \tag{3}$$

where  $d$  is the length of the F–P cavity, and  $n_e$  is the effective refractive index of the sensitive element in the F–P cavity. In general, the effective refractive index of calcium alginate hydrogel material (sensitive element) is about 1.334. The sensor also has an initial cavity length. When the sensor is immersed into a different methylene blue solution, the effective refractive index and volume (cavity length) of the calcium alginate hydrogel material will change because MB is adsorbed by calcium alginate, which will cause the change in optical path difference of F–P interference and eventually lead to the interference spectrum drift. The methylene blue concentration can be measured by measuring the interference spectrum drift.

## 2.2. Sensitive Materials

Hydrogel is a kind of polymer compound that can swell into a three-dimensional network structure in water and keep a lot of water without dissolution [31]. There are some special chemical groups in some hydrogels that are sensitive to external environment changes, such as ion concentration, temperature, pH value and electric field. [32]. When the external environment changes, the intermolecular forces change, and the molecular chains stretch or contract, resulting in changes in the gel volume. Such hydrogels are called smart hydrogels.

Sodium alginate (SA) is a natural water-soluble polyanionic polysaccharide that is prepared from seaweed [33] by extracting iodine and mannitol. It has excellent adsorption

properties for methylene blue and can be used as a sensitive material to measure the concentration of methylene blue [34]. The commonly used preparation methods for sodium alginate hydrogels include physical cross-linked hydrogels, chemical cross-linked hydrogels and enzyme cross-linked hydrogels. In this experiment, the physical cross-linking method is used to cross-link sodium alginate with calcium chloride solution to generate gel. In the aqueous solution of  $\text{CaCl}_2$ , SA and  $\text{Ca}^{2+}$  will quickly cross-link, and  $\text{Ca}^{2+}$  will be wrapped in the middle to form a quad-ligand structure, thus forming an “egg box model” [35]. Meanwhile,  $\text{Na}^+$  in SA will exchange with these bivalent cations to convert the SA solution to gel. The alginate group in the prepared calcium alginate hydrogel contains a lot of carboxyl groups, which can absorb methylene blue. The mass fraction of calcium chloride solution and sodium alginate solution is 2% in the experiment.

### 2.3. Experimental System

Figure 2 shows a schematic diagram of the experimental system. The high-precision optical fiber sensing analyzer (Micron Optics SM125) is connected to the computer for spectral data analysis. As a light source and spectrum measurement device, the Micron Optics SM125 fiber optic sensing analyzer provides 18 mW output optical power, 2 Hz scanning frequency, a scanning wavelength range of 1510–1590 nm and wavelength accuracy and stability of 1 pm. Figure 2c is the test area, which is composed of a fixing frame, optical fiber sensor and methylene blue solution. In experiments, the optical fiber sensor is fixed and immersed in the methylene blue solution. Figure 2d is the sensor diagram.

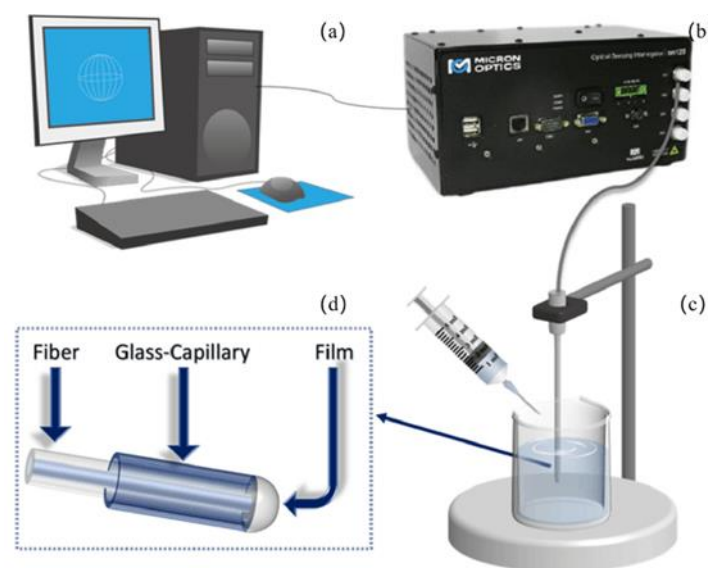


**Figure 2.** Methylene blue sensing experiment system (a) computer; (b) Micron Optics SM125; (c) test area; (d) sensor structure.

In experiments, the wavelength of light emitted by the SM125 is from 1510 nm to 1590 nm. The sensor was inserted into MB solutions with different concentrations. Using the spectrum data of different MB solutions, the relationship between the wavelength drift of interference and MB concentration was investigated.

## 3. Results and Discussions

### 3.1. Methylene Blue Response Experiments

In the methylene blue concentration-response experiments, the interference spectrum was measured with SM125. The spectrum data can be collected using MOI spectrum measurement software. The typical spectrum is shown in Figure 3a. The interference spectrum waveform has obvious peaks and valleys. This shape can be explained by the Formula (2). For testing the spectrum stability at a fixed concentration, the sensor

spectrum is monitored for 2000 s with SM125 at the initial conditions. The typical valley wavelength shift data of dip 1 in Figure 1b were focused to investigate the stability. This valley wavelength is near 1542 nm. According to the experimental data, the maximum valley wavelength shift of dip 1 was  $\pm 0.18$  nm. The response spectrum showed good stability, as Figure 3b shows. In follow-up experiments, we found that the sensor can keep a stable spectrum response for a longer time. We once tested one sensor every day for one week. The spectrum of the sensor was still good after the one-week test.

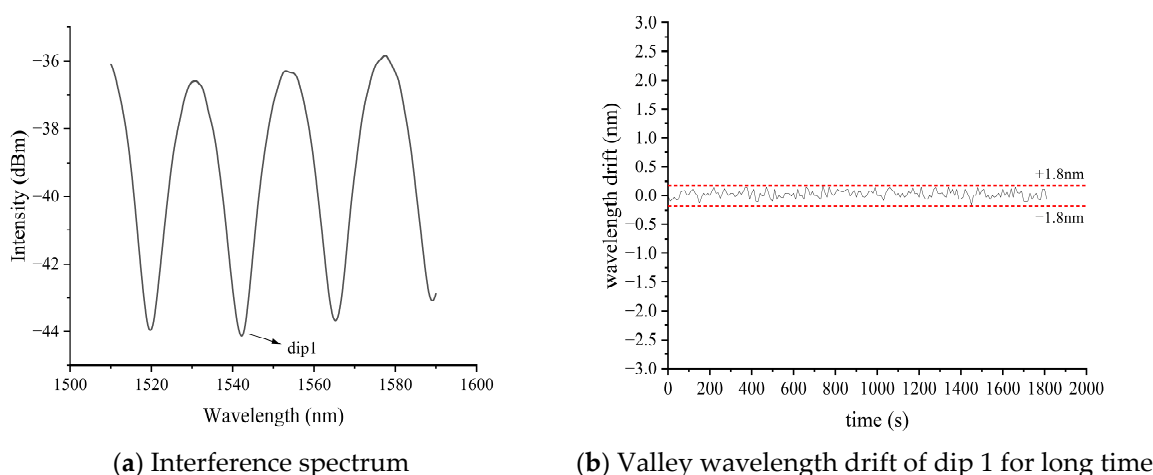


**Figure 3.** Response spectrum and stability measurement results.

For deeply investigating the response to methylene blue, we use many methylene blue solutions with different concentrations in experiments. Eleven methylene blue solutions with different concentrations are used in experiments, as Table 1 shows. The initial cavity length of the sensor is about 39.18  $\mu\text{m}$ . For sensitive materials preparations, the sodium alginate concentration is 2%. When the sensor is inserted into different MB solutions, the interference spectrum of the sensor will change according to the former discussion. The spectrum shape can be explained as Formula (2). The spectrum wave will drift left or right with different MB solution measurements. This is also observed in experiments. For the convenience of measurement and analysis, the peak or valley wavelength drift of the interference spectrum is focused for observation. The response is a kind of wavelength modulation because the spectrum peak or valley wavelength drifts with different concentrations of MB solution. The spectral data are recorded and saved with the SM125 and computer. Each measurement spectrum of different MB solutions is shown in Figure 4. With the increased methylene blue concentration, the peak wavelength obviously shifts to the left, as shown in Figure 4. This is caused by the optical path difference change, as formula (2) shows. To clearly show the wavelength drift, we chose the typical spectrum, the whole set of waves of dip 1, to gather in Figure 5. For the convenience of display, all curves of different concentrations are stacked together. We can see that the valley wavelength is about 1542 nm at 0 mg/L MB solution. When MB concentration increases, the valley wavelength of dip 1 changes obviously because the interference spectrum changes. For example, when the MB solution concentration is 10.70 mg/L, the valley wavelength is about 1515 nm. Compared with the wave of 0 mg/L, the valley wavelength is reduced by 27 nm.

**Table 1.** Methylene blue concentration list.

| Test Number                         | 1 | 2    | 3    | 4   | 5    | 6    | 7    | 8    | 9    | 10   | 11    |
|-------------------------------------|---|------|------|-----|------|------|------|------|------|------|-------|
| Methylene blue concentration/(mg/L) | 0 | 1.25 | 2.48 | 3.7 | 4.91 | 6.09 | 7.27 | 8.43 | 9.57 | 10.7 | 11.82 |

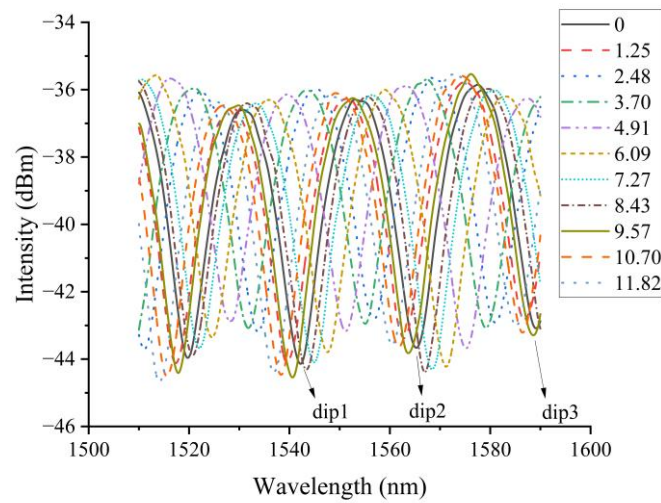


Figure 4. Sensor response spectrum with different methylene blue concentrations.

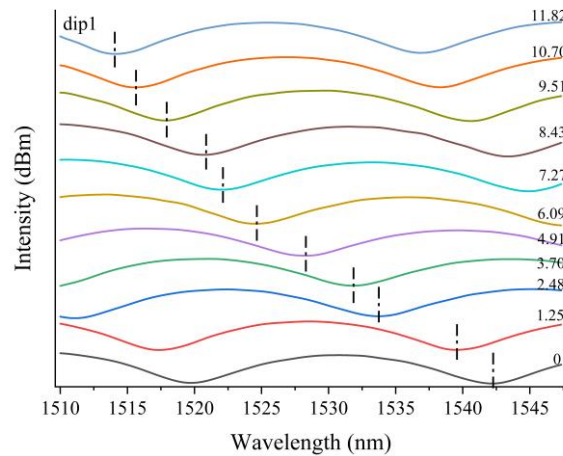


Figure 5. The wavelength shift of dip 1 trough.

The spectrum change is mainly due to the interaction of calcium alginate hydrogel with methylene blue, which changes the refractive index and cavity length. Therefore, the optical path difference between the two interference beams in the F–P cavity is changed, and the peak or valley wavelength is shifted. The obvious spectrum shift also shows an obvious response characteristic to the methylene blue concentration. The valley wavelength changes of the three dips (dip 1, dip 2, dip 3) in Figure 4 are monitored in experiments. The valley wavelength drift value is measured according to spectrum data. All wavelength drift values of the whole set of waves are listed in Table 2. The table shows each valley wavelength and its change with MB concentration. To reduce experimental errors, the average value of the three wavelength drift values is calculated for further analysis, as the last column in Table 2 shows. According to these spectral data in Table 2, the relationship curve between methylene blue concentration and average wavelength shift is obtained, as shown in Figure 6.

In the experiment, the wavelength shift of the interference spectrum was recorded. Some wave peaks or valleys may drift beyond the measurement range of the instrument. To avoid affecting the experimental results, special attention should be paid to peak drift during the experiment, and the spectral information should be recorded in time. As in the former discussion, we monitored three valley wavelengths, which can be measured in the measurement range of instruments.

As Figure 6 shows, there is a good linear relationship between the valley wavelength drift and methylene blue concentration. The linear fitting results show that its sensitivity is

2.46 nm/(mg/L), and the linear correlation coefficient is 0.99247. The experimental results show that the sensor has high response sensitivity and good linear response.

**Table 2.** Valley wavelength shift data.

| Methylene Blue Concentration/(mg/L) | dip1/nm | dip2/nm | dip3/nm | dip1-Shift/nm | dip2-Shift/nm | dip3-Shift/nm | Average Wavelength Drift/nm |
|-------------------------------------|---------|---------|---------|---------------|---------------|---------------|-----------------------------|
| 0                                   | 1589.09 | 1565.26 | 1542.15 | 0             | 0             | 0             | 0                           |
| 1.25                                | 1586.81 | 1562.84 | 1539.51 | 2.28          | 2.42          | 2.64          | 2.45                        |
| 2.48                                | 1580.98 | 1556.83 | 1533.73 | 8.11          | 8.43          | 8.42          | 8.32                        |
| 3.7                                 | 1579.13 | 1555.08 | 1531.81 | 9.96          | 10.18         | 10.34         | 10.16                       |
| 4.91                                | 1575.27 | 1551.15 | 1528.24 | 13.82         | 14.11         | 13.91         | 13.95                       |
| 6.09                                | 1571.26 | 1547.61 | 1524.54 | 17.83         | 17.65         | 17.61         | 17.70                       |
| 7.27                                | 1568.43 | 1544.84 | 1522.03 | 20.66         | 20.42         | 20.12         | 20.40                       |
| 8.43                                | 1566.97 | 1543.39 | 1520.71 | 22.12         | 21.87         | 21.44         | 21.81                       |
| 9.57                                | 1563.74 | 1540.61 | 1517.81 | 25.35         | 24.65         | 24.34         | 24.78                       |
| 10.7                                | 1561.79 | 1538.33 | 1515.52 | 27.3          | 26.93         | 26.63         | 26.95                       |
| 11.82                               | 1560.44 | 1536.86 | 1514.08 | 28.65         | 28.4          | 28.07         | 28.37                       |

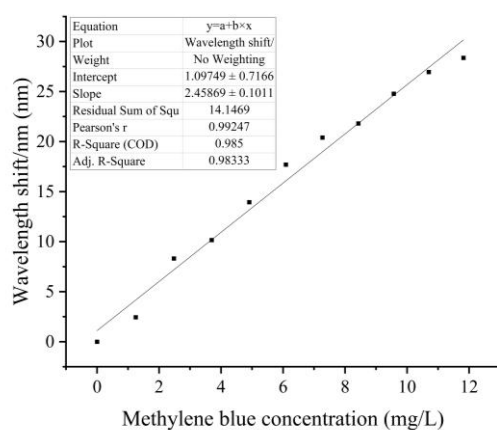


**Figure 6.** Valley wavelength shifts with different methylene blue concentrations.

### 3.2. Sodium Alginate Concentration Influence Investigation

As a sensitive material, the sensitive film can be formed by sodium alginate hydrogel. The sodium alginate hydrogel can be prepared with different concentrations. To investigate the sodium alginate concentration influence on response characteristics, five sensors with different sodium alginate concentrations are fabricated to test their response characteristics. The initial cavity length of each sensor is about 60 μm. The sodium alginate concentrations are 1.5%, 2%, 2.5%, 3% and 3.5%, respectively. For each sensor, the MB concentration response spectrum is measured with the same method as in Figure 6. So, we obtain five wavelength drift curves, as in Figure 6. Then, we gather all curves in one figure, and Figure 7 is attained. According to Figure 7, the spectrum valley wavelength shift of each sensor obviously increases with increased methylene blue concentration. The response sensitivities of the five sensors are 1.90 nm/(mg/L), 0.98 nm/(mg/L), 0.50 nm/(mg/L), 0.55 nm/(mg/L) and 0.43 nm/(mg/L), respectively. The response linearities of the five sensors are still good. The linear correlation coefficients of the five curves are 0.98388, 0.98801, 0.98658, 0.96186 and 0.97019, respectively.

According to the former discussion, five sensors have different sensitivities caused by different sodium alginate concentrations. Figure 8 is the relationship curve between the sensitivity and sodium alginate concentration. With increased sodium alginate concentration, the sensitivity curve first increased and then decreased. The concentration of about 2% is a turning point. It seems that the sodium alginate concentration has an optimum value for response sensitivity. This influence is caused by the swelling effect of the sensitive film. When the concentration of SA solution is too low, the strength of SA hydrogel microspheres is weak. The hydrogel film is difficult to form. The sensitive

film has a poor swelling effect and swelling ratio. When the SA concentration is gradually increased, a stable hydrogel film can be attained. The strength of SA hydrogel microspheres is strong enough to provide good swelling effects. But, the swelling effect cannot always remain strong when the SA solution concentration is higher. In the SA hydrogel preparation process, the gelation process of SA is an instantaneous ion exchange process between  $\text{Na}^+$  and  $\text{Ca}^{2+}$ . The high concentration of SA makes the intermolecular distance smaller. Then, some SA molecules inside the gel microspheres are formed before completely exchanging during the ion exchange process. Finally, the swelling ratio is reduced. A low swelling ratio will influence the MB molecule adsorption.

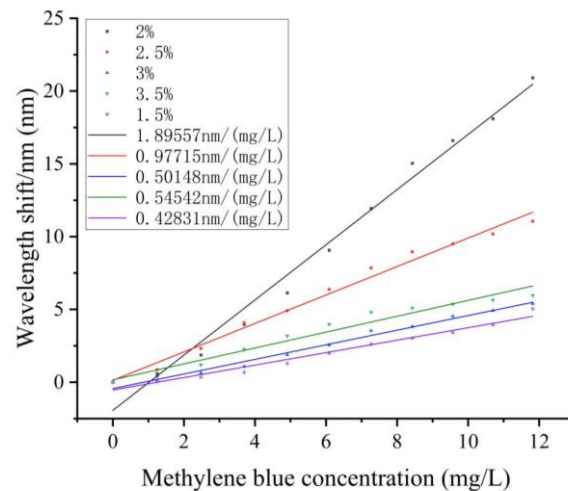


Figure 7. Valley wavelength shift of sensor spectrums with different sodium alginate concentrations.

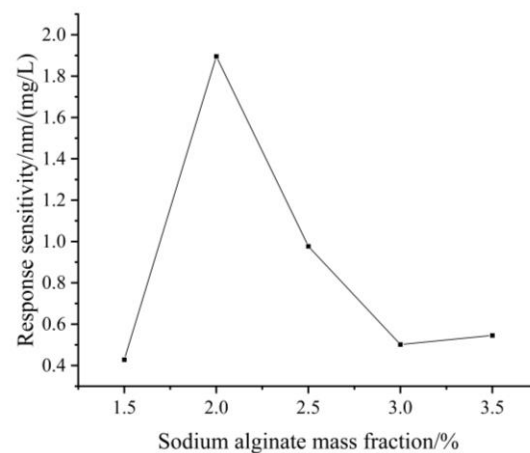


Figure 8. Response sensitivity of five sensors with different sodium alginate concentrations.

As far as we know, during the adsorption of MB in calcium alginate hydrogel,  $\text{—OH}$  and  $\text{—COOH}$  in the alginate group participate in the adsorption of MB. If the swelling ratio is high, the internal void is also large. This is more conducive to making the alginate group of the hydrogel coordinate with the methylene blue ion to the maximum extent.

So, for MB absorption, the SA solution has an optimum concentration to obtain an optimum swelling ratio of the hydrogel. According to our experimental results, about 2% is an optimum value, which is also consistent with the swelling experiment results of reference [36]. The curve-changing trends in Figure 8 can be explained, as in the former discussion.

### 3.3. Dynamic Response

The characteristic of dynamic response was also investigated. The Micron Optics SM125 measurement software of the computer is set to automatic acquisition mode at the acquisition frequency of 2 Hz. Then, SM125 continuously measures the spectrum data during the whole experiment. Firstly, we stood the sensor for five minutes to ensure the spectral stability and collected the interference spectrum data. Then, we inserted the sensor into a methylene blue solution with some concentration. The sensor was immersed in the solution for about ten minutes to record the stable spectrum. Then, we took out the sensor and immersed it in the next methylene blue solution with a different concentration. All spectral data were automatically recorded with SM125. Then, the next measurement of another concentration is repeated as before. In experiments, the concentration values are still the concentrations in Table 1. The initial cavity length of a typical sensor is 39.18  $\mu\text{m}$ . The sodium alginate concentration is still 2%.

Spectral data are processed and analyzed. The relationship between the peak wavelength shift and time is focused on spectral data processing. The dynamic response experimental curve is finally obtained, as Figure 9 shows. When the concentration of methylene blue in the environment changes, the peak wavelength shifts significantly. The curve presents a stepped shape because the peak wavelength shift of the spectrum increases with higher methylene blue concentrations.

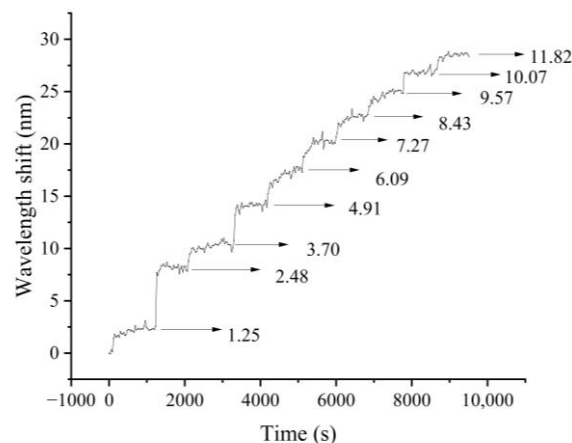


**Figure 9.** The dynamic peak wavelength shifts with different methylene blue concentrations.

To obtain more details of the dynamic response, we enlarged some curve details of Figure 9, as shown in Figure 10. According to this curve, the response time of the sensor is measured in the range from 10 to 90 percent of the wavelength drift range. When the methylene blue concentration increases from 1.25 mg/L to 2.48 mg/L, the response time is 25 s. The short response time implies that the sensor has a fast dynamic response.

### 3.4. Comparison with other Methylene Blue Sensors

To more deeply discuss the sensor characteristic, we compared our work with some reported methylene blue sensors. Table 3 shows the comparison between our work and some other reported methylene blue sensors. The sensors of references [19,37–39] 44 use electrochemical methods, which have complicated fabrication and measurement processes. The sensor of reference [27] has a wider measurement range, but it has lower response sensitivity and linearity. Compared with reference [40], our sensor has higher sensitivity and a shorter response time. The methylene blue concentration measurement range of references [28,41,42] is smaller than our work, and they use complex manufacturing processes or high-cost microstructure fibers. The sensor of our work has a simple structure and easy fabrication method. The sensitive material of our work is easy to prepare and very cheap. The sensor of reference [43] has a wider response range, but the linear response is not good. It uses complex microfabricated technology and a U-band waveguide. The

sensors of references [38,39,44] have longer response times and complex fabrications. The sensitive materials have complex preparation processes or high costs.

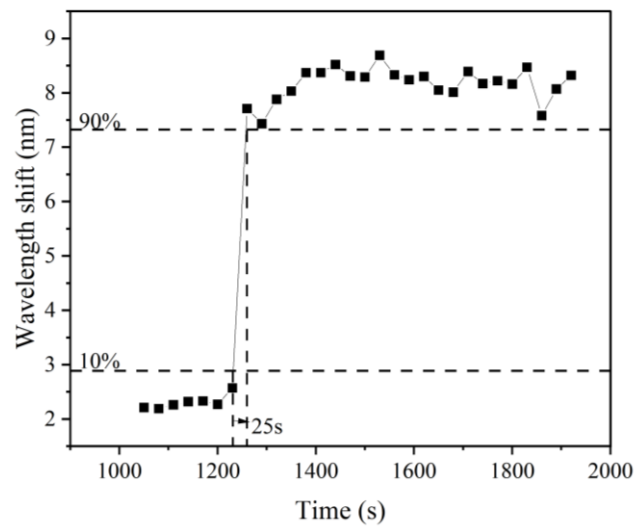


Figure 10. The enlarged view of typical dynamic response results.

Table 3. Comparison with other methylene blue sensors.

| Reference | Type                      | Fabrication  | Sensitive Materials  | Concentration Range (mg/L) | Sensitivity                         | Linearity                                | Response Time (s) |
|-----------|---------------------------|--|--|----------------------------|-------------------------------------|--|-------------------|
| [19]      | Electrochemical           | Long Period Fiber Grating                                      | Indium Tin Oxide   | 0.32–319.85                | \                                   | Not good (linear/logarithmic processing) | 60                |
| [27]      | Evanescent Field          | MEMS   | Silver Nanoparticle  | 0–127.94                   | 0.0126 dB/(mg/L)                    | 0.9496                                   | \                 |
| [28]      | Evanescent Field          | Cladless optical fiber   | \  | 6–10                       | 8.75 a.u/(mg/L)                     | \  | \                 |
| [37]      | Electrochemical           | Lossy mode Resonance (LMR) Fiber                               | Indium Tin Oxide   | 8.08–31.99                 | 2.66 (nm/V)/(mg/L)                  | 0.9714 (slope processing)                | \                 |
| [38]      | Electrochemical           | Quartz crystal microbalance                                    | MgFe <sub>2</sub> O <sub>4</sub> NPs/MgFe <sub>2</sub> O <sub>4</sub> @CaAlg NCs | 100–800                    | \                                   | \  | 300               |
| [39]      | Electrochemical           | Quartz crystal microbalance with dissipation monitoring        | Molecularly Imprinted Polymers   | 0.025–0.15                 | 1880.9 (ng/cm <sup>2</sup> )/(μg/L) | 0.9907                                   | 4000              |
| [40]      | Fluorescence spectrum     | \  | Carbon Quantum Dots (CQDs)   | 3.20–31.99                 | 0.0594/(mg/L)                       | 0.994                                    | 60                |
| [41]      | Evanescent Field          | HF etching /Less-mode optic fiber                              | \  | 0.11–0.79                  | \                                   | \  | \                 |
| [42]      | Evanescent Field          | Optical Fiber Tapers   | \  | 0.0016–0.31                | \                                   | Not good                                 | \                 |
| [43]      | Evanescent Field          | Microfabricated polymer chip with integrated U-bend waveguides | \  | 3.20–6397                  | \                                   | Not good                                 | \                 |
| [44]      | Surface plasmon resonance | \  | NiCo-Layered Double Hydroxide  | 0.005–10                   | \                                   | Not good                                 | 268               |
|           | Our work                  | Common Fiber   | Calcium Alginate Hydrogel  | 1.25–11.82                 | 2.46 nm/(mg/L)                      | 0.9824                                   | 25                |

Compared with these sensors, our sensor has high sensitivity, good response linearity, fast response time, easy fabrication and low cost. It provides a new convenient pathway to develop optical fiber methylene blue sensors. It has the potential to be applied to online methylene blue detection.

#### 4. Conclusions

In this paper, an optical fiber F–P cavity was constructed with a capillary glass tube, single-mode fiber and calcium alginate hydrogel film. We successfully prepared the calcium alginate hydrogel and fabricated the sensor. We built the experiment system to measure the sensor spectrum response to the methylene blue solution with different concentrations. A high response sensitivity to methylene blue concentration was verified in the range from 1.25 mg/L to 11.82 mg/L. The sensitivity of a typical sensor with a 39.18  $\mu\text{m}$  cavity length was 2.46 nm/(mg/L). The linearity of the experiment curve was 0.99247. The results implied that the sensor had high response sensitivity and good linear response characteristics. Furthermore, the sodium alginate concentration influence on sensitivity was investigated. The results show that the sodium alginate concentration of 2% is the optimum value to improve response sensitivity. Then, the dynamic response characteristics of the sensor were investigated. A total of 25 s of response time implied that the sensor has a fast dynamic response.

The research results show that this kind of optic fiber sensor in this paper has many advantages in methylene blue measurement, such as high sensitivity, good linearity, simple fabrication, low cost and fast response time. It can realize the direct response to methylene blue solutions of different concentrations. We believe that our study results will provide a new convenient pathway to design a methylene blue sensor. It has the development potential of in situ online monitoring of methylene blue pollution in water.

**Author Contributions:** Conceptualization, N.W. and W.L.; methodology, N.W. and S.L.; validation, N.W., W.L. and L.X.; formal analysis, W.L. and S.L.; investigation, N.W., W.L., L.W. and M.H.; writing—original draft preparation, N.W. and W.L.; writing—review and editing, N.W., W.L. and D.F.; supervision, N.W. All authors have read and agreed to the published version of the manuscript.

**Funding:** National Natural Science Foundation of China (No.61890964); Key Deployment Project of Ocean Science Research Center of Chinese Academy of Sciences (COMS2020 J11); National Training Program of Innovation and Entrepreneurship for Undergraduates (No. 202211033).

**Data Availability Statement:** The data underlying the presented results are not publicly available but may be obtained from the authors upon reasonable request.

**Conflicts of Interest:** The authors declare no conflict of interest regarding this article.

#### References

1. Oladoye, P.O.; Ajiboye, T.O.; Omotola, E.O.; Oyewola, O.J. Methylene Blue Dye: Toxicity and Potential Elimination Technology from Wastewater. *Results Eng.* **2022**, *16*, 100678. [[CrossRef](#)]
2. Erdem, A.; Kerman, K.; Meric, B.; Ozsoz, M. Methylene Blue as a Novel Electrochemical Hybridization Indicator. *Electroanalysis* **2001**, *13*, 219–223. [[CrossRef](#)]
3. Oz, M.; Lorke, D.E.; Hasan, M.; Petroianu, G.A. Cellular and Molecular Actions of Methylene Blue in the Nervous System. *Med. Res. Rev.* **2011**, *31*, 93–117. [[CrossRef](#)] [[PubMed](#)]
4. Auerbach, S.S.; Bristol, D.W.; Peckham, J.C.; Travlos, G.S.; Hébert, C.D.; Chhabra, R.S. Toxicity and Carcinogenicity Studies of Methylene Blue Trihydrate in F344N Rats and B6C3F1 Mice. *Food Chem. Toxicol.* **2010**, *48*, 169–177. [[CrossRef](#)]
5. Kishor, R.; Purchase, D.; Saratale, G.D.; Saratale, R.G.; Ferreira, L.F.R.; Bilal, M.; Chandra, R.; Bharagava, R.N. Ecotoxicological and Health Concerns of Persistent Coloring Pollutants of Textile Industry Wastewater and Treatment Approaches for Environmental Safety. *J. Environ. Chem. Eng.* **2021**, *9*, 105012. [[CrossRef](#)]
6. Rifci, L.M.; Cherry, D.S.; Farris, J.L.; Cairns, J. Acute and Subchronic Toxicity of Methylene Blue to Larval Fathead Minnows (*Pimephales Promelas*): Implications for Aquatic Toxicity Testing. *Environ. Toxicol. Chem.* **1996**, *15*, 1304–1308. [[CrossRef](#)]
7. Khan, I.; Saeed, K.; Zekker, I.; Zhang, B.; Hendi, A.H.; Ahmad, A.; Ahmad, S.; Zada, N.; Ahmad, H.; Shah, L.A.; et al. Review on Methylene Blue: Its Properties, Uses, Toxicity and Photodegradation. *Water* **2022**, *14*, 242. [[CrossRef](#)]
8. Kolomaznik, K.; Adamek, M.; Andel, I.; Uhlirova, M. Leather Waste—Potential Threat to Human Health, and a New Technology of Its Treatment. *J. Hazard. Mater.* **2008**, *160*, 514–520. [[CrossRef](#)]

9. Xu, T.; Wang, X.; Huang, Y.; Lai, K.; Fan, Y. Rapid Detection of Trace Methylene Blue and Malachite Green in Four Fish Tissues by Ultra-Sensitive Surface-Enhanced Raman Spectroscopy Coated with Gold Nanorods. *Food Control* **2019**, *106*, 106720. [[CrossRef](#)]
10. Li, X.; Lin, L.; Chiang, W.H. Microplasma synthesized gold nanoparticles for surface enhanced Raman spectroscopic detection of methylene blue. *React. Chem. Eng.* **2022**, *7*, 346–353. [[CrossRef](#)]
11. Zhang, X.; Hui, Y.; Fang, C.; Wang, Y.; Han, F.; Lou, X.; Fodjo, E.K.; Cai, Y.; Kong, C. Determination of Methylene Blue and Its Metabolite Residues in Aquatic Products by High-Performance Liquid Chromatography–Tandem Mass Spectrometry. *Molecules* **2021**, *26*, 4975. [[CrossRef](#)] [[PubMed](#)]
12. Hayat, M.; Shah, A.; Nisar, J.; Shah, I.; Haleem, A.; Ashiq, M.N. A Novel Electrochemical Sensing Platform for the Sensitive Detection and Degradation Monitoring of Methylene Blue. *Catalysts* **2022**, *12*, 306. [[CrossRef](#)]
13. Bahrololoomi, A.; Bilan, H.K.; Podlaha, E.J. Electrodeposited Ni-Fe onto Glassy Carbon for the Detection of Methylene Blue. *J. Electrochem. Soc.* **2022**, *169*, 012501. [[CrossRef](#)]
14. Matsuhisa, K.; Ohzeki, K.; Kambara, T. Coagulated Ion-exchanger Colorimetry for the Determination of Trace Amounts of Sulfide as Methylene Blue. *Bull. Chem. Soc. Jpn.* **1983**, *56*, 3847–3848. [[CrossRef](#)]
15. Xu, Y.-J.; Tian, X.-H.; Zhang, X.-Z.; Gong, X.-H.; Liu, H.-H.; Zhang, H.-J.; Huang, H.; Zhang, L.-M. Simultaneous Determination of Malachite Green, Crystal Violet, Methylene Blue and the Metabolite Residues in Aquatic Products by Ultra-Performance Liquid Chromatography with Electropray Ionization Tandem Mass Spectrometry. *J. Chromatogr. Sci.* **2012**, *50*, 591–597. [[CrossRef](#)]
16. Kalmár, J.; Lente, G.; Fábrián, I. Kinetics and Mechanism of the Adsorption of Methylene Blue from Aqueous Solution on the Surface of a Quartz Cuvette by On-Line UV–Vis Spectrophotometry. *Dye. Pigment.* **2016**, *127*, 170–178. [[CrossRef](#)]
17. Ashok, K.E.; Jiann, W.T.; Chang, Y.-H. Ultrasensitive SERS Substrates Based on Au Nanoparticles Photo-Decorated on Cu<sub>2</sub>O Microspheres for the Detection of Rhodamine B and Methylene Blue. *Appl. Surf. Sci.* **2022**, *585*, 152696. [[CrossRef](#)]
18. Zahran, M.; Khalifa, Z.; Zahran, M.A.-H.; Azzem, M.A. Gum Arabic-Capped Silver Nanoparticles for Electrochemical Amplification Sensing of Methylene Blue in River Water. *Electrochim. Acta* **2021**, *394*, 139152. [[CrossRef](#)]
19. Okazaki, T.; Orii, T.; Tan, S.-Y.; Watanabe, T.; Taguchi, A.; Rahman, F.A.; Kuramitz, H. Electrochemical Long Period Fiber Grating Sensing for Electroactive Species. *Anal. Chem.* **2020**, *92*, 9714–9721. [[CrossRef](#)]
20. Liu, T. Fibre Optic Sensors for Coal Mine Hazard Detection. In *Handbook of Optical Fibers*; Peng, G.-D., Ed.; Springer: Singapore, 2018; pp. 1–27. [[CrossRef](#)]
21. Nascimento, M.; Ferreira, M.S.; Pinto, J.L. Real Time Thermal Monitoring of Lithium Batteries with Fiber Sensors and Thermocouples: A Comparative Study. *Measurement* **2017**, *111*, 260–263. [[CrossRef](#)]
22. Alwis, L.; Sun, T.; Grattan, K.T.V. Optical Fibre-Based Sensor Technology for Humidity and Moisture Measurement: Review of Recent Progress. *Measurement* **2013**, *46*, 4052–4074. [[CrossRef](#)]
23. Memon, S.F.; Ali, M.M.; Pembroke, J.T.; Chowdhry, B.S.; Lewis, E. Measurement of Ultralow Level Bioethanol Concentration for Production Using Evanescent Wave Based Optical Fiber Sensor. *IEEE Trans. Instrum. Meas.* **2018**, *67*, 780–788. [[CrossRef](#)]
24. Chen, L. Construction and Signal Feature Processing of Gold Nanobiosensors Based on the Internet of Things. *J. Healthc. Eng.* **2022**, *2022*, 1432266. [[CrossRef](#)] [[PubMed](#)]
25. Cai, S.; Pan, H.; González-Vila, Á. Selective detection of cadmium ions using plasmonic optical fiber gratings functionalized with bacteria. *Opt. Express* **2020**, *28*, 19740–19749. [[CrossRef](#)] [[PubMed](#)]
26. Coelho, L.; De Almeida, J.M.M.M.; Santos, J.L.; Ferreira, R.A.S.; André, P.S.; Viegas, D. Sensing Structure Based on Surface Plasmon Resonance in Chemically Etched Single Mode Optical Fibres. *Plasmonics* **2015**, *10*, 319–327. [[CrossRef](#)]
27. Luo, J.; Yao, J.; Lu, Y.; Ma, W.; Zhuang, X. A Silver Nanoparticle-Modified Evanescent Field Optical Fiber Sensor for Methylene Blue Detection. *Sensors* **2013**, *13*, 3986–3997. [[CrossRef](#)]
28. Azil, K.; Ferria, K.; Bouzid, S. Cladless Optical Fiber Sensor Based on Evanescent Wave Absorption for Monitoring Methylene Blue Induced Water Pollution. *J. Opt. Soc. Am. B* **2020**, *37*, A253. [[CrossRef](#)]
29. Yin, X.; Wang, N.; Yu, X. Theoretical Analysis and Optimization of Extrinsic Fabry–Perot Interferometer Optical-fiber Humidity-sensor Structures. *Curr. Opt. Photon.* **2021**, *5*, 652–659. [[CrossRef](#)]
30. Santos, J.S.; Raimundo, I.M.; Cordeiro, C.M.B.; Biazoli, C.R.; Gouveia, C.A.J.; Jorge, P.A.S. Characterisation of a Nafion Film by Optical Fibre Fabry–Perot Interferometry for Humidity Sensing. *Sens. Actuators B Chem.* **2014**, *196*, 99–105. [[CrossRef](#)]
31. Jindrich, K. Polymer chemistry: Swell gels. *Nature* **2002**, *417*, 15419–15425. [[CrossRef](#)]
32. Mahinroosta, M.; Jomeh Farsangi, Z.; Allahverdi, A.; Shakoobi, Z. Hydrogels as Intelligent Materials: A Brief Review of Synthesis, Properties and Applications. *Mater. Today Chem.* **2018**, *8*, 42–55. [[CrossRef](#)]
33. Ma, Y.-X.; Li, X.; Shao, W.-J.; Kou, Y.-L.; Yang, H.-P.; Zhang, D.-J. Fabrication of 3D Porous Polyvinyl Alcohol/Sodium Alginate/Graphene Oxide Spherical Composites for the Adsorption of Methylene Blue. *J. Nanosci. Nanotechnol.* **2020**, *20*, 2205–2213. [[CrossRef](#)] [[PubMed](#)]
34. Wang, C.; Feng, X.; Shang, S. Lignin/sodium alginate hydrogel for efficient removal of methylene blue. *Int. J. Biol. Macromol.* **2023**, *237*, 124200. [[CrossRef](#)] [[PubMed](#)]
35. Yu, J.; Wang, Y.; He, Y.; Gao, Y.; Hou, R.; Ma, J.; Zhang, L.; Guo, X.; Chen, L. Calcium Ion-Sodium Alginate Double Cross-Linked Graphene Oxide Nanofiltration Membrane with Enhanced Stability for Efficient Separation of Dyes. *Sep. Purif. Technol.* **2021**, *276*, 119348. [[CrossRef](#)]
36. Zhang, C.Y. *Preparation and Applications of pH-Sensitive Calcium Alginate Porous Hydrogel Microsphere*; Dalian University of Technology: Dalian, China, 2010.

37. Okazaki, T.; Yoshioka, M.; Orii, T.; Taguchi, A.; Kuramitz, H.; Watanabe, T. Electrochemical Lossy Mode Resonance-based Fiber Optic Sensing for Electroactive Species. *Electroanalysis* **2023**, *35*, e202200089. [[CrossRef](#)]
38. Al-Gethami, W.; Al-Qasbi, N.; Ismail, S.H.; Sadek, A.H. QCM-Based MgFe<sub>2</sub>O<sub>4</sub>@CaAlg Nanocomposite as a Fast Response Nanosensor for Real-Time Detection of Methylene Blue Dye. *Nanomaterials* **2022**, *13*, 97. [[CrossRef](#)] [[PubMed](#)]
39. Hu, Y.; Xing, H.; Li, G.; Wu, M. Magnetic Imprinted Polymer-Based Quartz Crystal Microbalance Sensor for Sensitive Label-Free Detection of Methylene Blue in Groundwater. *Sensors* **2020**, *20*, 5506. [[CrossRef](#)]
40. Vyas, T.; Gogoi, M.; Joshi, A. Fluorescent-fiber optic device sensor based on Carbon Quantum dots (CQD) thin films for dye detection in water resources. *Analyst* **2023**, *148*, 5178–5189. [[CrossRef](#)]
41. Wu, Y.; Deng, X.; Li, F.; Zhuang, X. Less-Mode Optic Fiber Evanescent Wave Absorbing Sensor: Parameter Design for High Sensitivity Liquid Detection. *Sens. Actuators B Chem.* **2007**, *122*, 127–133. [[CrossRef](#)]
42. Gravina, R.; Testa, G.; Bernini, R. Perfluorinated Plastic Optical Fiber Tapers for Evanescent Wave Sensing. *Sensors* **2009**, *9*, 10423–10433. [[CrossRef](#)]
43. Prabhakar, A.; Mukherji, S. Microfabricated Polymer Chip with Integrated U-Bend Waveguides for Evanescent Field Absorption Based Detection. *Lab. Chip* **2010**, *10*, 748. [[CrossRef](#)] [[PubMed](#)]
44. Sadrolhosseini, A.R.; Ghasemi, E.; Pirkarimi, A.; Hamidi, S.M.; Taheri Ghahrizjani, R. Highly Sensitive Surface Plasmon Resonance Sensor for Detection of Methylene Blue and Methylene Orange Dyes Using NiCo-Layered Double Hydroxide. *Opt. Commun.* **2023**, *529*, 129057. [[CrossRef](#)]

**Disclaimer/Publisher's Note:** The statements, opinions and data contained in all publications are solely those of the individual author(s) and contributor(s) and not of MDPI and/or the editor(s). MDPI and/or the editor(s) disclaim responsibility for any injury to people or property resulting from any ideas, methods, instructions or products referred to in the content.